JOURNAL OF GEOPHYSICAL RESEARCH, VOL. 105, NO. C3, PAGES 6493–6499, MARCH 15, 2000

Spectral reflectance of whitecaps: Their contribution to water-leaving radiance

Karl D. Moore, Kenneth J. Voss, and Howard R. Gordon
Physics Department, University of Miami, Coral Gables, Florida

Abstract. A radiometric system, deployed from a ship, is used to measure directly the influence of the presence of breaking waves (whitecaps) on the upwelling radiance above the sea surface. Estimates of their remote sensing augmented spectral reflectance, i.e., the temporally averaged or spatially averaged increase in the ocean's reflectance over and above the reflectance in the absence of breaking waves, are provided from measurements in the tropical Pacific. The accuracy of these estimates is dependent on their ability to determine radiometrically the background reflectance of the water. In the visible the remote sensing augmented spectral reflectance of whitecaps measured in the open ocean was found to be essentially independent of wavelength and in the range 0.001–0.002 for wind speeds of 9–12 m s^{-1}. This is in reasonably good agreement (within a factor of 2) with earlier predictions based on the statistical relationship between fractional coverage and wind speed and the estimated average reflectance of individual whitecaps. In the near infrared (860 nm) the remote sensing augmented spectral reflectance falls to ~80% of its value in the visible.

1. Introduction

Because of the relatively small radiance backscattered into the atmosphere from below the ocean surface (the water-leaving radiance) in comparison to the total light arriving at a space-borne ocean color sensor, the usefulness of ocean color data depends primarily on the accuracy of atmospheric correction algorithms [*Gordon and Morel*, 1983]. Atmospheric correction over the ocean is effected by measurement of the upwelling signal arriving at the satellite at spectral bands where the radiance backscattered out of the ocean is known to contribute very little or no signal [*Gordon and Wang*, 1994a]. Utilization of spectral bands beyond ~740 nm in case 1 waters, i.e., waters in which the optical properties are determined by phytoplankton, their decay products, and the water itself [*Gordon and Morel*, 1983] can be justified in the absence of whitecaps because of the strong absorption properties of liquid water in the near infrared (NIR). When waves break on the sea surface, the presence of the resulting whitecaps occurring within a satellite image pixel increases the radiometric signal by an amount dependent on the whitecap coverage and its reflectance. This increase in apparent surface reflectance over and above that in the absence of breaking waves is referred to here as the augmented reflectance. (In this paper we consider whitecaps to be any near-surface manifestation that results from breaking waves. Such manifestations include what could be called subjectively "thick foam" (a lattice of bubbles floating on the sea surface), "thin foam" (a single layer of bubbles on the surface), and "subsurface bubbles" (air injected into the water during the breaking process). They do not include surface roughness normally associated with "Sun glitter." Historically, the whitecap coverage (or fractional coverage) was usually taken to be the fraction of the sea surface covered by thick foam.) Previous researchers have used a whitecap reflectance of 50–100% [*Payne*, 1972; *Maul and Gordon*, 1975; *Gordon and Jacobs*, 1977] and have assumed it to be constant at all wavelengths. Laboratory measurements carried out by *Whitlock et al*. [1982] yielded a value of ~55% in the visible part of the spectrum for thick foam in clear water and showed that it diminishes with increasing wavelength beyond ~0.8 μm, with a 5% decrease at 0.85 μm, 10% at 1.02 μm, and 50% at 1.65 μm. *Koepke* [1984] determined the effective reflectance of whitecaps to be 22% in the visible, taking into consideration the decrease in reflectance and increase in area of an individual whitecap as it ages. He then combined this wavelength-independent estimate of the effective reflectance with the fractional area of the sea surface covered with whitecaps as a function of wind speed [*Monahan and O'Muircheartaigh*, 1980] to obtain the overall reflectance of whitecaps for different wind speeds. Using Koepke's model for the reflectance as a function of wind speed and the *Whitlock et al*. [1982] spectral variation of foam reflectance, *Gordon and Wang* [1994b] carried out simulations suggesting that adequate atmospheric correction of ocean color sensors could be made at wind speeds ~10–12 m s^{-1} even in the presence of large errors (approximately a factor of 2) in estimating the contribution to the sensor radiance due to whitecaps.

Recently, field measurements of the reflectance of foam generated by breaking waves in the surf zone [*Frouin et al*., 1996] indicated a larger spectral variation in reflectance than was reported by *Whitlock et al*. [1982]. *Frouin et al*. [1996] found that the reflectance decreased by 40% at 0.87 μm, 50% at 1.02 μm, and 95% at 1.65 μm relative to the reflectance at 440 nm. The greater spectral variation in reflectance found in their field data, when compared to the laboratory foam measurements of Whitlock et al., is thought to be due to the strong absorption properties of water at the longer wavelengths. This absorption attenuates light reflected from submerged bubbles that are forced into the water column by the breaking waves. Using the spectral variation reported by *Frouin et al*. [1996], *Gordon* [1997] recomputed their influence on atmospheric cor-

Paper number 1999JC900334.
0148-0227/00/1999JC900334$09.00

rection and found whitecaps to be a far more serious problem than was reported by *Gordon and Wang* [1994b].

In addition to the spectral differences between foam measured in the laboratory and in the field, estimates of whitecap fractional coverage for different wind speeds are found to be extraordinarily noisy [*Blanchard*, 1971; *Monahan*, 1971; *Ross and Cardone*, 1974; *Wu*, 1979; *Toba and Chaen*, 1973; *Monahan and O'Muircheartaigh*, 1980, 1986], with the mean fractional coverage, for a given wind speed, and its standard deviation being roughly the same. Typically, fractional coverage W has been related to wind speed U through an equation of the form $W = \alpha U^{\beta}$. The values of α and β vary with geographic location, air and sea temperature, and wind speed range. These relationships remain noisy, despite attempts to fine tune particular data sets, because of the dynamic nature and interdependence of the many parameters involved in whitecap formation. Whitecap coverage is primarily dependent on wind speed but is also dependent on other factors such as fetch and duration [*Cardone*, 1969], water temperature [*Miyake and Abe*, 1948], air temperature, stability of the lower atmosphere defined by the air/water temperature differential [*Monahan and O'Muircheartaigh*, 1986], salinity [*Monahan and Zietlow*, 1969], and even surface tension variations due to the presence of organic films [*Garrett*, 1967]. A slightly different approach by *Wu* [1988] relates whitecap coverage to the product of wind friction velocity and wind stress. *Bortkovskii and Novak* [1993] assessed whitecap and foam coverage with particular dependence on the sea surface temperature, which affects sea water viscosity and wind friction.

To date the influence of whitecaps on the upwelling water-leaving radiance has been estimated by utilizing and combining the work of different researchers as described above. In this paper a measurement system deployed from a ship is used to determine directly the augmented spectral reflectance resulting from the presence of breaking waves on the sea surface. Our measurement system provides spectral reflectance data from individual whitecaps in various stages of growth and decay. By integrating over time, estimates of the augmented spectral reflectance relevant to remote sensing can be determined. We undertook the present investigation for two reasons: (1) to see if the *Frouin et al*. [1996] spectral measurements in a highly productive surf zone were applicable to real oceanic whitecaps and (2) to validate the whitecap reflectance versus wind speed relationship developed by *Koepke* [1984] and proposed for application to ocean color sensors [*Gordon and Wang*, 1994b].

2. Instrument System

The whitecap reflectance measurement system is described in detail elsewhere [*Moore et al*., 1998]. The system consists of a six-channel radiometer with a narrow field of view and bands with nominal 10 nm spectral width centered at 410, 440, 510, 550, 670, and 860 nm. It is held over the water surface by means of a boom extended from the bow of a ship, providing an unobstructed view of the water surface. The field of view (FOV) of an individual channel on the sea surface is ~14 cm in diameter. Simultaneously, a deck unit with a cosine collector and matching spectral bands measures downwelling irradiance so that the reflectance of the water surface can be calculated. A television camera is mounted next to the radiometer to provide a visual reference. Whenever the radiometric data are acquired, the associated video frame is time and date marked and recorded onto videotape to assist in later analysis. Air and water temperature and wind speed and direction are measured simultaneously with the radiometric data at a rate of ~7 s^{-1} continuously for ~30 s (providing 200 contiguous samples), after which Global Positioning System (GPS) data, universal time, and location are recorded. This acquisition sequence is repeated until a time determined by the operator. This radiometric rate allows several sample points of a large individual whitecap to be captured as well as provides an adequate data set over a time period of reasonably constant sea state and sky conditions. However, note that for a ship speed of 10 kts (5 m s^{-1}) the samples are ~70 cm apart, so the radiometer will rarely view the same area of the ocean surface twice.

Once the system has been installed on a ship, only periodic measurements of the detector dark current are necessary. This requires bringing the radiometer in from the boom and covering both the radiometer and the deck cell with light tight caps. This is necessary only when significant temperature changes are encountered such as when conditions change from early morning to noon or from dark, overcast, rainy conditions to bright sunshine. The radiometer can also be angled up to 20° from nadir in order to minimize the effects of specular Sun and sky glitter.

The purpose of the video camera was to remove events attributable to Sun glitter from the analysis. Unfortunately, separating whitecaps from Sun glitter was much more difficult than had been anticipated and usually could not be done accurately. Thus most of the data reported here were acquired under overcast conditions (no Sun glitter).

3. Data Description

Data used in this paper are from a ~6000 km transit through equatorial waters of the Pacific Ocean from Manzanillo, Mexico (19.03°N, 104.20°W), to Honolulu, Hawaii (21.20°N, 157.55°W). This 13 day cruise took place in November 1996 abroad the National Oceanic and Atmospheric Association (NOAA) ship R/V *Ka'imimoana*. Conditions were uniform with air/water temperature and wind speed/direction changing only by a relatively small amount over time. Fetch was typically >1000 km, and duration could be considered unlimited. Data were acquired far from land, and for the most part, water temperature was ~22°–23°C with air temperature ~20°–23°C. Wind speeds ranged from ~8 to ~13 m s^{-1}, and wind direction changed from an initial northerly direction at the beginning of the transect to an easterly and southerly direction as the trade winds were crossed. Wind speed was constant within 1–2 m s^{-1} for days at a time. The sky conditions were mainly broken and scattered cloudiness with some overcast periods. The data used in the analysis were collected under overcast conditions during 3 days of the transect. Reflectance data were acquired for wind speeds between ~9 and 12 m s^{-1}. Stability of the lower atmosphere, defined by the air temperature/water temperature differential, varied from neutral to slightly unstable.

4. Data Reduction Procedure

The radiometric data collected were reduced to produce detector dark current–corrected and radiometrically corrected reflectance values R from the six upwelling and downwelling channels. This reflectance is defined as $R(\lambda) = \pi L(\lambda)/E(\lambda)$, where $L(\lambda)$ is the upward radiance leaving the sea surface and $E(\lambda)$ is the downward irradiance falling onto the sea surface

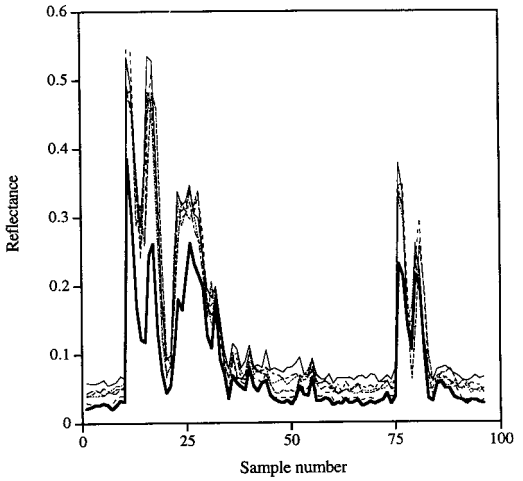

Figure 1a. An ~15 s record of the reflectance of two whitecaps passing within the field of view of the radiometer. The thick line corresponds to 860 nm.

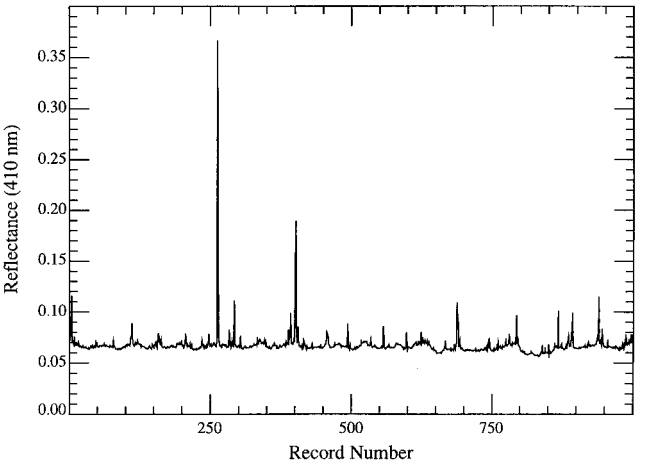

Figure 1b. Time series of the reflectance of the sea surface at 410 nm. The record covers 1000 samples, and the sampling rate is 7 Hz.

from the Sun and sky. If the surface were lambertian (L independent of the viewing direction), then R would be the surface albedo. The radiometric correction process consists of three steps [*Moore et al*., 1998] briefly reviewed here.

First, ratios of upwelling radiance to downwelling irradiance are formed from the detector dark current–corrected signals for each channel. These six ratios are then multiplied by a radiometric absolute calibration factor relating the channels in the radiometer to those in the deck cell. This was established using a calibrated 1000 W (FEL) quartz halogen lamp source and a calibrated Spectralon reflectance plaque. The deck cell was positioned 50 cm in front of the source, and measurements were taken. For the radiometer the reflectance plaque replaced the deck cell, and the radiometer viewed the plaque at a 45° angle. One obtains the desired relationship by noting that (apart from a small correction for the departure of the plaque from lambertian) the radiance of the plaque is $\pi R E_0$, where E_0 is the irradiance falling on the plaque (the same as the irradiance falling on the deck cell) and R is the reflectance of the plaque. Second, a multiplicative factor was used to correct for spectral differences between the radiometer and deck cell and for differences between laboratory and field spectral illumination conditions [*Moore et al*., 1998]. Third, each channel of the deck cell was corrected for solid angle response for operation under natural illumination due to the slight deviation in angular response of the deck cell collector from a true cosine response. Correction factors for different angular distributions of the downwelling light field are required for the various sky conditions that may be encountered. A set of correction factors were established for sky conditions, such as overcast or clear with different solar zenith angles, to correct solid angle response [*Moore et al*., 1998].

After applying these corrections we are left with a time series of spectral reflectance from the sea surface, examples of which are shown in Figures 1a and 1b. Figure 1a provides a 15 s record of the reflectance of two whitecaps passing within the radiometer FOV during an earlier deployment of the instrument in the Gulf of Mexico. It shows (1) that all spectral channels have essentially the same view of this whitecap, (2) that the reflectance of the whitecaps throughout the visible is essentially independent of wavelength, and (3) that the whitecap reflectance at 860 nm is significantly lower than that in the visible, in agreement with the surf zone observations of *Frouin et al*. [1996]. Figure 1b shows a longer record of the reflectance at 410 nm obtained in the Pacific deployment.

We wish to estimate the augmented reflectance [AR(λ)] associated with each whitecap event recorded in the time series. To discriminate automatically whitecaps and foam from the background reflectance, we filtered each data set. The filter works in three steps on each wavelength individually. An example of the process steps is shown in Figure 2. Because whitecaps are associated with rapid changes in the surface reflectance, the first step is to determine the data points for which the reflectance has changed by ±0.001 from the previous data point. For these data points we believe there is a whitecap (or whitecap fragment) in the radiometer FOV. After this process is complete and candidate whitecaps have been determined, the background surface and subsurface reflectance must be eliminated. For each whitecap event we subtract the average of the first nonwhitecap data point before and after

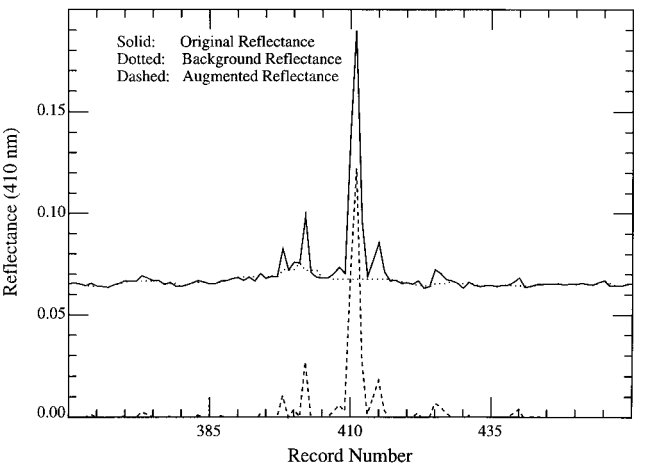

Figure 2. Sample record from Figure 1b showing the operation of the filter at 410 nm. The solid line is the recorded surface reflectance. The dotted line is the background reflectance (reflectance in the absence of the whitecap). The dashed line is the augmented reflectance.

the event (step 2 of the filter). We are then left with individual cases of the enhanced reflectance (the augmented reflectance) due to the whitecap event. (This subtraction process inevitably leads to a few events with small negative augmented reflectance; however, their contribution to the final result will be negligible.) Finally, we eliminate the events for which the augmented reflectance is <0.01. This last step, referred to as a threshold, is somewhat arbitrary; however, it results in fractional coverage estimates that are similar to those found by other investigators for similar wind speeds [e.g., *Monahan*, 1971]. We will discuss the implications of this step below. Because the Fresnel surface reflectance is a much higher portion of the total reflectance for the red channels, the data are significantly noisier (especially at 860 nm), and this procedure is much less reliable in the red than in the blue channels. This filtering procedure was validated by comparing the video record and the radiometric record. The filter (without the threshold test) passes candidate events that we subjectively consider to be whitecaps; however, it also can pass events that are only associated with changes in reflected skylight (due to the rough nature of the surface). These latter events are completely removed by the thresholding test. Thus, employing only steps 1 and 2, the contribution to the reflectance due to breaking waves will be overestimated. Using the threshold test (step 3) reduces this overestimation and, in fact, may underestimate their contribution somewhat.

Within the context of ocean color remote sensing the remote sensing augmented reflectance (RSAR(λ)) is simply the increase in the water-leaving reflectance (averaged over a single pixel, typically ~1 km^2) due to the presence of breaking waves on the surface. If the remote sensor had sufficient spatial resolution, one could, in principle, measure RSAR(λ) by subtracting the radiance measured in whitecap-free areas from the radiance averaged over a large number of pixels that include whitecaps and open water, after accounting for the transmission loss in the atmosphere. RSAR is then the average reflectance that the whitecaps have added to the surface reflectance.

We attempt to effect the same determination at 410 nm by replacing the spatial average over ~1 km^2 by the time average of AR(410) over an ~14 cm diameter circle on the sea surface. The remote sensing augmented reflectance at 410 nm was determined from the radiometer record by taking the sum of AR(410) for the reflectance "events" that passed these filters (Figure 2) and dividing by the total number of records. Using the events that passed steps 1 and 2 of the filter provides an upper limit to RSAR(410) because examination of the video record shows that events are passed that (subjectively) are not associated with whitecaps. These nonwhitecap events are removed (possibly along with some whitecap-associated events) by the threshold in step 3. Computation of RSAR(410) for the events that passed all three steps of the filter produces a lower limit to the augmented reflectance; however, as comparison with the video record indicated that the first two steps of the filter often passed nonwhitecap events, we believe that the lower limit is closer to the actual augmented reflectance.

We can estimate the fractional coverage W by simply taking the ratio of the number of records containing events to the total number of records. This estimate will be higher than previous estimates (based on photography [*Monahan*, 1971; *Koepke*, 1984]) for two reasons: (1) steps 1 and 2 of the filter pass events that are not whitecaps; that is, any event that changes AR by 0.001 is passed; and (2) if a small whitecap is detected but does not fill the radiometer FOV, it will be included in the estimate of W as if it did fill the FOV. For the wind speeds observed here (9–12 m s^{-1}), W was ~30% for events that passed steps 1 and 2 but fell to ~2–3% for events that passed the threshold as well. This latter range for W is more consistent with earlier estimates for these wind speeds and suggests that the implementation of all three steps of the filter should provide results that are consistent with the subjective definition of whitecaps used in earlier studies based on photography.

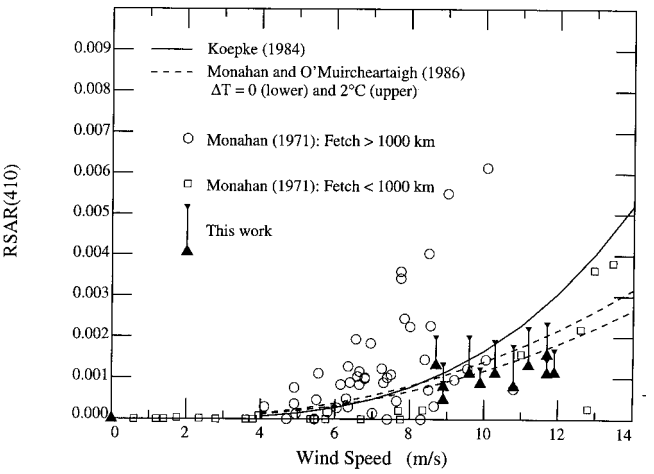

Figure 3. Remote-sensing augmented reflectance of whitecaps at 410 nm. The large solid triangles are our measurements for whitecap events that have passed all three steps of the filter. The small solid triangles are our measurements for events that have passed steps 1 and 2 of the filter (no threshold). The open symbols are the *Monahan* [1971] fractional coverages multiplied by 0.155, the *Koepke* [1984] effective whitecap reflectance of 0.22 minus 0.065 to convert from reflectance to augmented reflectance. The upper solid line is the *Koepke* [1984] whitecap reflectance model converted to augmented reflectance: RSAR = $4.57 \times 10^{-7}\, U^{3.52}$. The dashed lines use the *Monahan and O'Muircheartaigh* [1986] model for a neutrally stable atmosphere ($\Delta T = 0$, lower dashed line) and an unstable atmosphere ($\Delta T = 2C$, upper dashed line) to provide the fractional coverage for use in computing the augmented reflectance: RSAR = $3 \times 10^{-6}\, U^{2.55} \exp(0.0861 \times \Delta T)$.

In Figure 3 we present RSAR(410), as a function of wind speed, resulting from the analysis of 11 data sets. Each of the 11 data points was for an average acquisition time of 45 min. Values of RSAR(410) that result from employing all three steps of the filter are indicated by the large solid triangles. RSAR(410) for the zero threshold case (using only the first two steps of the filter) is shown in Figure 3 as our upper limit (small solid triangles). Figure 3 indicates that our measurements show virtually no dependence of RSAR on wind speed. This behavior is compared with the RSAR versus wind speed relationships computed for several whitecap models in Figure 3. The solid line is the *Koepke* [1984] model with the effective whitecap reflectance reduced from 0.22 to 0.22–0.065 (to convert from Koepke's total reflectance to our augmented reflectance). The dashed lines use the same reduced effective reflectance and the *Monahan and O'Muircheartaigh* [1986] model for $\Delta T = 0°$ and 2°C. The individual points use the *Monahan* [1971] measurements of fractional coverage and the reduced effective reflectance. The *Monahan and O'Muircheartaigh* [1986] model is seen to fit our data better than the *Koepke*

[1984] model. Possible correlations between the RSAR and other parameters such as water temperature, air temperature, stability of the lower atmosphere, humidity, salinity, barometric pressure, wave height, and sea swell were investigated, but none could be established mainly because the small variation in the parameters during the transect. We believe that the null dependence of RSAR on wind speed seen in our data is the result of the small range in wind speeds that we encountered during the measurements.

The filter scheme did not work reliably for the red wavelengths because of excessive fluctuations in the background, so another technique was used to determine the spectral variation of AR(λ). This was accomplished by passing the record for the wavelength λ through the first two steps of the filter and comparing the result with the record for the 410 nm band passed through all three steps of the filter. If the filtered 410 nm band record indicated a whitecap, its augmented reflectance along with the augmented reflectance of the same event in the λ band were recorded. Figure 4 compares the values of AR(λ) and AR(410) for individual events for one of the records that we examined. For each λ (except 860 nm) the line on Figure 4 is a 1:1 line. The noisy appearance Figures 4a–4e is partially due to the fact that each channel looks at a slightly different part of the surface. The anomalous behavior of the 550 nm band at low reflectance compared to the others is probably due to a larger misalignment for this band than the others. Clearly, for all channels (except 860 nm) the data fall near the 1:1 line. For 860 nm the line shown is a least squares fit (to an exponential) of the data. It clearly follows the 1:1 line reasonably well for low AR; however, for large AR, AR(860) is significantly less than AR(410). The depression of AR(860) at large values is similar to that noted by *Frouin et al*. [1996] for breaking surf zone waves and by *Moore et al*. [1998] for ship wakes (also see Figure 1a). Clearly, this analysis suggests that the reflectance of whitecaps at 860 nm decreases relative to that in the visible and that the fractional decrease is greater at larger AR(λ); that is, AR(860)/AR(λ) decreases as AR(λ) increases. The brightest whitecaps (here AR(λ) ~ 0.3) show a reflectance decrease of ~50% from the visible to 860 nm.

Using the exponential relationship between AR(860) and AR(410) shown in Figure 4, we can compute RSAR(860) for an entire record using AR(410) for each event to find AR(860) and averaging AR(860) over the record. The result is that for the range 9–12 m s^{-1}, RSAR(860)/RSAR(410) ≈ 0.8, with the ratio decreasing slightly as the wind speed increases. As the wind speed increases, the occurrence of larger whitecaps increases. These larger whitecaps individually have the lowest ratio of AR(860 nm)/AR(410 nm), which lowers the overall ratio RSAR(860)/RSAR(410) for that wind speed.

5. Concluding Remarks

We have determined the remote sensing augmented reflectance of whitecaps in the open ocean for the 410–670 nm spectral region to be 0.001–0.002 over the wind speed range 9–12 m s^{-1}. These values are somewhat lower than previously derived values of whitecap optical influence (Figure 3) and show no obvious dependence on wind speed. We believe this lack of dependence on wind speed is due to the narrow range encountered in our measurements and the inherent uncertainty in our analysis. Using the *Koepke* [1984] effective reflectance of 22% (minus 6.5% to convert from total reflectance to RSAR) and the fractional coverage determined by wind speed for water temperature above 14°C [*Monahan and O'Muircheartaigh*, 1980] yields values that are approximately twice our values near 12 m s^{-1}. (However, one should note that Koepke places a ±11% uncertainty on the effective reflectance; that is, his effective reflectance could be from 11 to 33%.) Applying the fractional coverage relationship, which takes into account atmospheric stability [*Monahan and O'Muircheartaigh*, 1986], our results are in reasonable agreement with Monahan and O'Muircheartaigh's for a stable atmosphere (Figure 3) over the limited range of wind speeds we have examined. As there is much historical data relating whitecap fractional coverage to wind speed and the RSAR should be roughly proportional to the fractional coverage, to extend the measurements beyond the range of our data (for remote sensing purposes), we adopt the *Monahan and O'Muircheartaigh* [1986] model (for a stable atmosphere) to relate RSAR to U using our measurements to set the values of the parameters. Taking RSAR at 412 nm to be ~0.0012 for $U = 10$ m s^{-1} (Figure 3) we have

$$\mathrm{RSAR}(412) = 3.4 \times 10^{-6} U^{2.55},$$

where U is in m s^{-1}. This provides a better fit to our data than the *Koepke* [1984] model.

Our measurements of individual whitecaps clearly show that the reflectance in the NIR is depressed compared to the visible (Figure 1a) and that the depression increases as AR(410) increases (Figure 4e). This depression is in agreement with the measurements of *Frouin et al*. [1996] in the surf zone. Quantitatively, converting their measurements to AR (by subtracting off the background given by *Frouin et al*. [1996, Figure 1]), their AR depression is 30–35%, while our results show a depression in RSAR of ~20% for wind speeds of 9–12 m s^{-1} in the open ocean. This suggests that the less violent wave breaking manifest in the open ocean at these wind speeds on the average does not inject bubbles to as great a depth as wave breaking in the surf zone; however, for individual whitecap events with large AR(410) we have observed significant depression in the NIR compared to the visible (Figure 4e), and this is likely characteristic of violent breaking.

The goal of this study was to determine the augmented reflectance from whitecaps as viewed from satellites and its spectral dependence. Although most of our open ocean analysis utilized only data acquired during overcast conditions (to eliminate Sun glint), some data for partly cloudy and clear skies were examined. This partly cloudy/clear-sky data appeared to be similar to the overcast cases; however, its analysis carried far more uncertainty because of our inability to separate clearly Sun glint from whitecaps in the video record. Unlike specular reflection from the sea surface, we expect that the augmented reflectance of whitecaps (which is closer to diffuse reflection) should be similar under clear and cloudy conditions and believe that our RSAR results should be reasonably representative of clear-sky situations and useful for estimating the whitecap contribution to the reflectance measured by ocean color sensors.

An earlier version of the results presented here (utilizing a different, and we believe less precise, method of analysis) is presently being used to process SeaWiFS imagery. It replaced the original *Koepke* [1984] reflectance versus wind speed relationship (as interpreted by *Gordon and Wang* [1994b]) with one that reduced the RSAR for a given wind speed by a factor of 4. This improved the processing at high wind speeds, particularly in the South Atlantic (C. R. McClain, Goddard Space

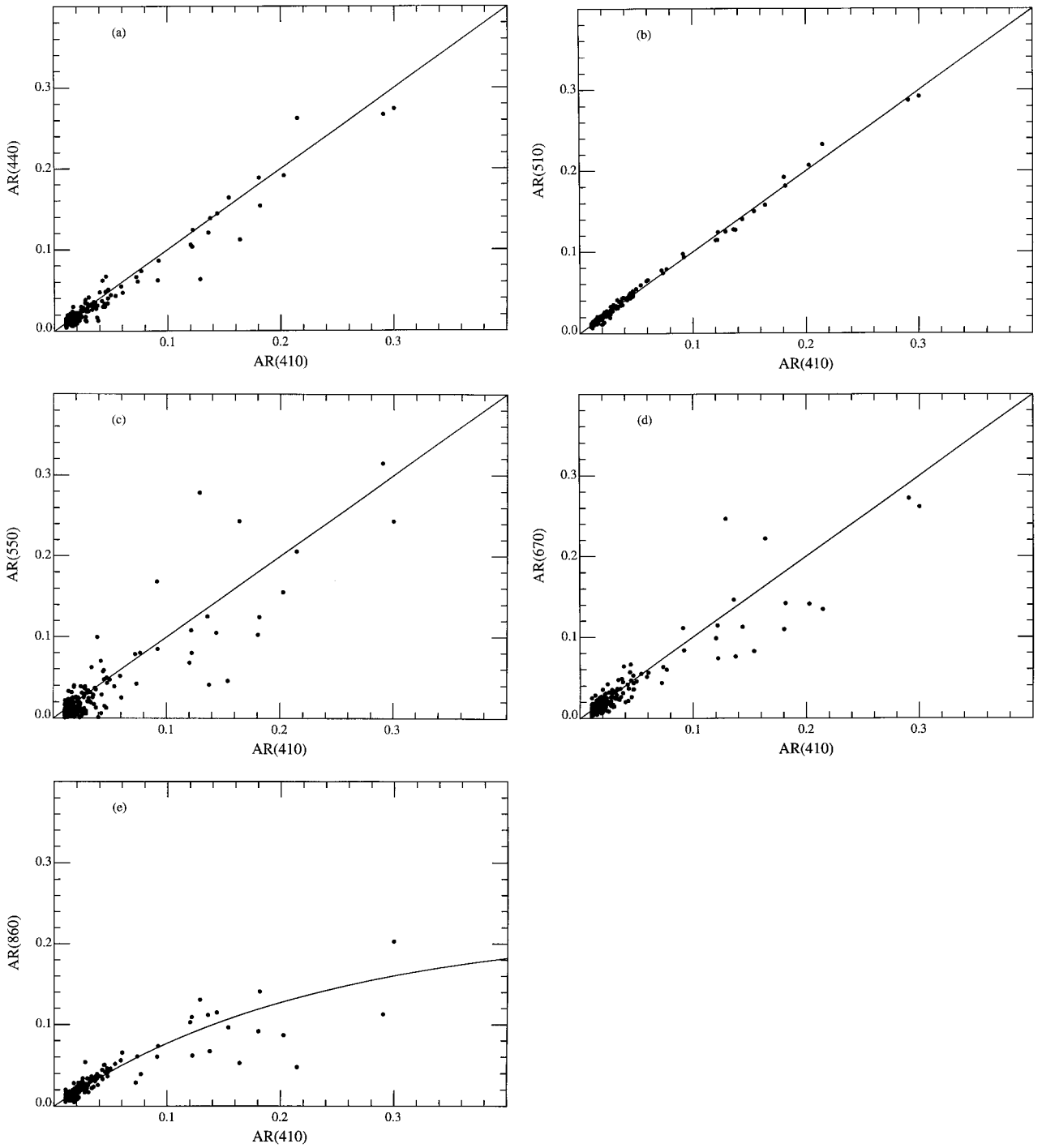

Figure 4. Comparison of AR(λ) and AR(410) for individual whitecap events: (a) AR(440) versus AR(410); (b) AR(510) versus AR(410); (c) AR(550) versus AR(410); (d) AR(670) versus AR(410); and (e) AR(860) versus AR(410). The solid lines on all graphs (except AR(860) versus AR(410)) are 1:1 lines. For the AR(860) versus AR(410) graph, the curve is given by $AR(860) = 0.22\{1 - \exp[-4.2AR(410)]\}$.

Flight Center, personal communication, 1998). The revised version presented here is proposed for future processing.

Notation

AR(λ)	augmented reflectance at wavelength λ.
RSAR(λ)	remote sensing–augmented reflectance at wavelength λ.
T_{air}	air temperature.
T_{water}	water surface temperature.
ΔT	temperature differential ($\Delta T = T_{water} - T_{air}$).
U	wind speed in meters per second.
W	fractional coverage of whitecaps and foam.

Acknowledgments. This research was funded by NASA/EOS-MODIS, Goddard Space Flight Center under contract NAS5-31363. We would like to thank Al Chapin for his help in the design and construction of the equipment and Cecil Williams for helping in the

validation of the digital filter. We would like to thank the NOAA personnel Mark Koehn, Tim Wright, John Herring, and Michael McPhaden for allowing us to join their transit aboard the R/V *Ka'imimoana*. We are grateful to R. Frouin for pointing out an error in our interpretation of the *Koepke* [1984] reflectance as RSAR. The same error was made by *Gordon and Wang* [1994b].

References

Blanchard, D. C., Whitecaps at sea, *J. Atmos. Sci*., *28*, 645, 1971.

Bortkovskii, R. S., and V. A. Novak, Statistical dependencies of sea state characteristics on water temperature and wind-wave age, *J. Mar. Syst*., *4*, 161–169, 1993.

Cardone, V. J., Specification of the wind field distribution in the marine boundary layer for wave forecasting, *Rep. TR 69-1*, Geophys. Sci. Lab., New York Univ., New York, 1969.

Frouin, R., M. Schwindling, and P. Y. Deschamps, Spectral reflectance of sea foam in the visible and near infrared: In situ measurements and remote sensing implications, *J. Geophys. Res*., *101*, 14,361–14,371, 1996.

Garrett, W. D., The influence of surface-active material on the properties of air bubbles at the air/sea interface, *Rep. 6545*, 14 pp., Naval Res. Lab., Washington, D. C., 1967.

Gordon, H. R., Atmospheric correction of ocean color imagery in the Earth Observing System era, *J. Geophys. Res*., *102*, 17,081–17,106, 1997.

Gordon, H. R., and M. M. Jacobs, Albedo of the ocean-atmosphere system: Influence of sea foam, *Appl. Opt*., *16*, 2257–2260, 1977.

Gordon, H. R., and A. Morel, *Remote Assessment of Ocean Color for Interpretation of Satellite Visible Imagery*: *A Review*, Springer-Verlag, New York, 1983.

Gordon, H. R., and M. Wang, Retrieval of water-leaving radiance and aerosol optical thickness over the oceans with SeaWiFS: A preliminary algorithm, *Appl. Opt*., *33*, 443–452, 1994a.

Gordon, H. R., and M. Wang, Influence of oceanic whitecaps on atmospheric correction of SeaWiFS, *Appl. Opt*., *33*, 7754–7763, 1994b.

Koepke, P., Effective reflectance of oceanic whitecaps, *Appl. Opt*., *23*, 1816–1824, 1984.

Maul, G. A., and H. R. Gordon, On the use of Earth resources technology satellite (LANDSAT-1) in optical oceanography, *Remote Sens. Environ*., *4*, 95–128, 1975.

Miyake, Y., and T. Abe, A study on the foaming of sea water, *J. Mar. Res*., *7*, 67–73, 1948.

Monahan, E. C., Oceanic whitecaps, *J. Phys. Oceanogr*., *1*, 139–144, 1971.

Monahan, E. C., and I. G. O'Muircheartaigh, Optimal power-law description of oceanic whitecap coverage dependence on wind speed, *J. Phys. Oceanogr*., *10*, 2094–2099, 1980.

Monahan, E. C., and I. G. O'Muircheartaigh, Whitecaps and passive remote sensing of the ocean surface, *Int. J. Remote Sens*., *7*, 627–642, 1986.

Monahan, E. C., and C. R. Zietlow, Laboratory comparisons of fresh-water and salt-water whitecaps, *J. Geophys. Res*., *74*, 6961–6966, 1969.

Moore, K. D., K. J. Voss, and H. R. Gordon, Spectral reflectance of whitecaps: Instrumentation, calibration and performance in coastal waters, *J. Atmos. Oceanic Technol*., *15*, 496–509, 1998.

Payne, R. E., Albedo of the sea surface, *J. Atmos. Phys*., *29*, 959–970, 1972.

Ross, D. B., and V. J. Cardone, Observations of oceanic whitecaps and their relation to remote measurements of surface wind speed, *J. Geophys. Res*., *79*, 444–452, 1974.

Toba, Y., and M. Chaen, Quantitative expression of the breaking of wind waves on the sea surface, *Rec. Oceanogr. Works Jpn*., *12*, 1–11, 1973.

Whitlock, C. H., D. S. Bartlett, and E. A. Gurganus, Sea foam reflectance and influence on optimum wavelength for remote sensing of ocean aerosols, *Geophys. Res. Lett*., *9*, 719–722, 1982.

Wu, J., Oceanic whitecaps and sea state, *J. Phys. Oceanogr*., *9*, 1064–1068, 1979.

Wu, J., Variation of whitecap coverage with wind stress and water temperature, *J. Phys. Oceanogr*., *18*, 1448–1453, 1988.

H. R. Gordon, K. D. Moore, and K. J. Voss, Physics Department, University of Miami, Coral Gables, FL 33124.

(Received June 25, 1999; revised November 23, 1999;
accepted November 30, 1999.)